Structure and magnetism of well defined cobalt nanoparticles embedded in a niobium matrix

M. Jamet, V. Dupuis, P. Mélinon, G. Guiraud, and A. Pérez
Département de Physique des Matériaux, Université Claude Bernard-Lyon 1 et CNRS, 69622 Villeurbanne, France

W. Wernsdorfer
Laboratoire Louis Néel, CNRS, 38042 Grenoble, France

A. Traverse
LURE, CNRS CEA MENJS, Bâtiment 209A, BP 34, 91898 Orsay, France

B. Baguenard
Laboratoire de Spectrométrie ionique et moléculaire, Université Claude Bernard Lyon 1 et CNRS, 69622 Villeurbanne, France
(Received 22 December 1999)

Our recent studies on Co clusters embedded in various matrices reveal that the co-deposition technique (simultaneous deposition of two beams: one for the preformed clusters and one for the matrix atoms) is a powerful tool to prepare magnetic nanostructures with any couple of materials even though they are miscible. We study both structure and magnetism of the Co/Nb system, which are intimately related. Because such a heterogeneous system needs to be described at different scales, we used microscopic and macroscopic techniques, and in addition local element selective probes based on x-ray absorption. We conclude that our clusters are 3-nm-diameter fcc truncated octahedrons with a pure cobalt core and a solid solution between Co and Nb located at the interface which could be responsible for the magnetically inactive monolayers we found.

I. INTRODUCTION

Structural and magnetic properties of clusters, i.e., particles containing from two to a few thousand atoms, are of great interest nowadays. From a technological point of view, those systems are part of the development of high-density magnetic storage media, and, from a fundamental point of view, the physics of magnetic clusters still needs to be investigated. Indeed, to perform stable magnetic storage with small clusters, one has to control the magnetization reversal process (nucleation and dynamics), and thus make a close connection between structure and magnetic behavior. To reach the magnetic properties of small clusters, there are two available approaches: ''macroscopic'' measurements [using a vibrating sample magnetometer (VSM) or a superconducting quantum interference device (SQUID)] on a cluster collection (10^9 particles) that implicate statistical treatments of the data, and ''microscopic'' measurements on a single particle. From now, micromagnetometers [MFM,[1] Hall microprobe,[2] or classical micro-SQUID (Ref. 3)] were not sensitive enough to perform magnetic measurements on a single cluster. The present paper constitutes the preliminary study toward magnetic measurements on a small single cluster using a new micro-SQUID design. We focus on and try to connect structural and magnetic properties of a cluster collection. With a view to clear up structural questions, we first study the structure of nanocrystalline Co particles embedded in a niobium matrix by means of transmission electron microscope (TEM) observations, x-ray diffraction, and absorption techniques. Then magnetization measurements are performed on the same particles to deduce their magnetic size and their anisotropy terms.

II. EXPERIMENTAL DEVICES

We use the co-deposition technique recently developed in our laboratory to prepare the samples.[4] It consists in two independent beams reaching at the same time a silicon (100) substrate at room temperature: the preformed cluster beam and the atomic beam used for the matrix. The deposition is made in an ultrahigh vacuum (UHV) chamber ($p=5\times10^{-10}$ Torr) to limit cluster and matrix oxidation. The cluster source used for this experiment is a classical laser vaporization source improved according to Milani–de Heer design.[5] It allows us to work in the low-energy cluster beam deposition (LECBD) regime: clusters do not fragment arriving on the substrate or in the matrix.[6] The vaporization Ti:sapphire laser used provides output energies up to 300 mJ at 790 nm, in a pulse duration of 3 μs and a 20-Hz repetition rate. It presents many advantages described elsewhere,[7] such as adjustable high cluster flux. The matrix is evaporated thanks to a UHV electron gun in communication with the deposition chamber. By monitoring and controlling both evaporation rates with quartz balances, we can continuously adjust the cluster concentration in the matrix. We previously show that this technique allows us to prepare nanogranular films from any couple of materials, even two miscible ones forbidden by the phase diagram at equilibrium.[8] We determine the crystalline structure and the morphology of cobalt clusters deposited onto copper grids and protected by a thin carbon layer (100 Å). From earlier high-resolution transmission electron microscopy (HRTEM) observations, we found that cobalt clusters form quasispherical nanocrystallites with a fcc structure, and a sharp size distribution.[9,4] In order to perform macroscopic measurements on a cluster collection using surface sensitive techniques, we need films having a

5–25-nm equivalent thickness of cobalt clusters embedded in 500-nm-thick niobium films. We chose a low cluster concentration (1–5 %) to make structural and magnetic measurements on noninteracting particles. One has to mention that such concentration is still far from the expected percolation threshold (about 20%).[4] From both x-ray reflectometry and grazing x-ray scattering measurements, we measured the density of the Nb films: 92% of the bulk one, and a bcc polycrystalline structure as reported for common bulk. X-ray absorption spectroscopy (XAS) was performed on D42 at the LURE facility in Orsay using the x-ray beam delivered by the DCI storage ring[10] at the Co *K* edge (7709 eV) by electron detection at low temperature ($T=80$ K).[11] The porosity of the matrix is low enough and avoids the oxidation of the reactive Co clusters as shown in x-ray appearance near-edge structure (XANES) spectra at the Co-*K* edge where no fingerprint of oxide on cobalt clusters embedded in niobium films is observed. The results of the extended x-ray absorption fine-structure (EXAFS) simulations reveal the local distances between first Co neighbors and their number for each component. Magnetization measurements on diluted samples were performed using a vibrating sample magnetometer (VSM) at the Laboratoire Louis Néel in Grenoble. Other low-temperature magnetization curves of the same samples were obtained from x-ray magnetic circular dichroism (XMCD) signal. The measurement was conducted at the European Synchrotron Radiation Facility in Grenoble at the ID12B beamline. The degree of circular polarization was almost 80%, and the hysteresis measurements were performed using a helium-cooled UHV electromagnet that provided magnetic fields up to 3 T.

III. STRUCTURE

The origin of the EXAFS signal is well established as mentioned in various references.[12] If multiple scattering effects are neglected on the first nearest neighbors, the EXAFS modulations are described in terms of interferences between the outgoing and the backscattered photoelectron wave functions. We use McKale tabulated phase and amplitude shifts for all types of considered Co neighbors.[13] The EXAFS analysis is restricted to solely simple diffusion paths from the standard fitting code developed in the Michalowicz version[14] where an amplitude reduction factor S_0^2 equal to 0.7 (Ref. 15) and an asymmetric distance distribution based on hard sphere model[16] are introduced. The first consideration traduces the possibility of multiple electron excitations contributing to the total absorption coefficient reduction. The second one is needed to take into account the difference between the core and the interface Co-atom distances in the cluster.[9] So, in the fit, R_j and s_j values, corresponding to the shortest distance and to the asymmetry parameter of the jth atom from the excited one, respectively, replace the average distance in the standard EXAFS formulation. We also define N_j the coordination number, σ_j the Debye-Waller factor of the jth atom, k the photoelectron momentum, and $\Gamma(k)$ its mean free path. Structural parameters $(N_j, R_j, \sigma_j, s_j)$ were determined from the simulation of the EXAFS oscillations (Fig. 1). As for some systems with two components (for example, in metallic superlattices previously studied[10,17]), the first Fourier transform peak of the EXAFS spectrum presents a shoulder which can be understood unambiguously in terms of phase shift between Co and Nb backscatterers for k values around 5 Å^{-1}. This splitting in the real space corresponds to a broadening of the second oscillation in the momentum space[10] (see Fig. 1). Thus, in the simulations, we first consider two kinds of Co neighbors: cobalt and niobium. But a preliminary study of cobalt and niobium core levels by x-ray photoelectron spectroscopy reveals a weak concentration of oxygen inside the sample owing to the UHV environment. The core level yielding provides an oxygen concentration of about 5%. Such Co-O bonding is taken into account for the fit improvement. Moreover, from HRTEM and x-ray-diffraction patterns,[4,9] we know: the mean size of the clusters (3 nm), their inner fcc structure with a lattice parameter close to the bulk one, and their shape close to the Wulff equilibrium one (truncated octahedron). Finally, the Co/Nb system can be usefully seen as a cobalt core with the bulk parameters and a more or less sharp Co/Nb interface. From these assumptions, we use the simulation of EXAFS oscillations to describe the Co/Nb interface and to verify it is relevant with an observed alloy in the phase diagram (tetragonal Co_6Nb_7). The best fitted values of EXAFS oscillations are the following:

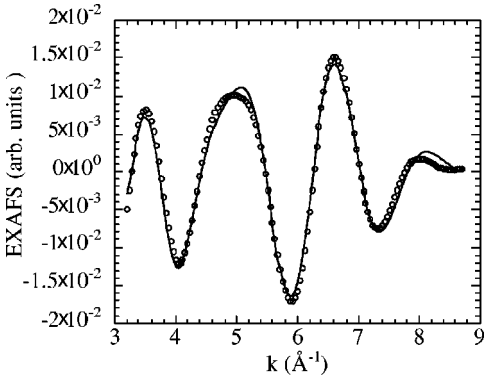

FIG. 1. EXAFS spectrum obtained on the sample containing 5% of cobalt clusters embedded in niobium (○: experimental data, continuous line: simulation).

(i) 70% of Co atoms are surrounded with cobalt neighbors in the fcc phase with the bulklike distance ($d_{Co-Co}=2.50$ Å), corresponding to $N_1=8.4$, $R_1=2.495$ Å, $\sigma_1=0.1$ Å, $s_1=0.18$ Å in EXAFS simulations.

(ii) 26% of Co atoms are surrounded with niobium neighbors in the tetragonal Co_6Nb_7 phase, corresponding to $N_2=3.1$, $R_2=2.58$ Å, $\sigma_2=0.16$ Å, $s_2=0.06$ Å in EXAFS simulations.

(iii) 4% of Co atoms are surrounded with oxygen neighbors with a distance equal to $d_{Co-O}=2.0$ Å based on the typical oxygen atomic radii in chemisorption systems[18] or transition-metal oxides. This environment corresponds to $N_3=0.5$, $R_3=1.9$ Å, $\sigma_3=0.04$ Å, $s_3=0.1$ Å in EXAFS simulations.

According to Ref. 19, a 3-nm-diameter fcc truncated octahedron consists of 35.6% core atoms (zone a), 27% atoms in the first sublayer (zone b), and 37.6% atoms in the surface layer (zone c). Let us propose the following compositions: a pure fcc Co phase in zone a, a Co_4Nb phase in zone b, and a $Co_6Nb_7O_2$ phase in zone c (i.e., at the cluster-matrix interface). The corresponding coordination numbers:

N_1(Co-Co)=8.5, N_2(Co-Nb)=3.1, and N_3(Co-O)=0.4 are in good quantitative agreement with the coordination numbers N_1, N_2, and N_3 we obtain from EXAFS simulations. Concerning the other fitting parameters, what is found is the high value for the mean free path of the photoelectron ($\Gamma=1.6$) and the Debye-Waller factor for Co-metal environment ($\sigma>0.1$ Å). Notice that because we did not dispose of experimental phase and amplitude, but calculated ones, a large difference between sample and reference is expected, so their absolute values do not represent physical reality but only are necessary to attenuate the amplitude of oscillations. On the contrary, the total number of neighbors is fixed by TEM experiments which reveal a fcc phase for the Co clusters (so $N_1+N_2+N_3=11\pm1$). To follow the shape, position, and relative amplitudes of the oscillations, N_j is a free parameter for each component in the simulation and besides is related to the concentration of the jth atom from the Co absorber one in the sample. This study finally evidences a diffuse interface between cobalt and niobium mostly located on the first monolayer.

In summary, we made a consistent treatment of all the experimental results obtained from different techniques. We notice that EXAFS spectra show unambiguously a smooth interface between miscible elements as cobalt and niobium. This information will be of importance and is the key to understand the magnetic behavior discussed below.

IV. MAGNETISM

Here, we present the magnetic properties of these nanometer sized clusters embedded in a metallic matrix. Furthermore, such a system will be used to perform micro-SQUID devices in order to reach magnetization measurements on an isolated single domain cluster. The present study deals with macroscopic measurements performed on a particle assembly (typically 10^{14}) of cobalt clusters in a niobium matrix to describe the magnetic properties of the Co/Nb system. Because of the goal mentioned above, we focus on very diluted samples (less than 2% volumic for Co concentrations). For these low cluster concentrations, magnetic couplings between particles are negligible whereas dipolar and Ruderman-Kittel-Kasuya-Yosida (RKKY) interactions in the case of metallic matrix, are considered. Nevertheless, both last contributions which vary as $1/d_{ij}^3$ (where d_{ij} is the mean distance between particles) are expected to be weak compared to ferromagnetic order inside the cluster. In a first approximation, we neglect any kind of surface disorder so that a single domain cluster can be seen as an isolated macrospin with uniform rotation of its magnetization. It means that the atomic spins in the cluster remain parallel during the cluster magnetization rotation. In an external applied field, the magnetic energy of a nanoparticle is the sum of a Zeeman interaction (between the cluster magnetization and the local field), and anisotropy terms [as shape, magnetocrystalline, surface (interface in our case), or strain anisotropy]. At high temperatures ($T>100$ K), anisotropy contributions of nanometric clusters can be neglected compared to the thermal activation [$K_{eff}V/k_B\approx30$ K (Ref. 20)] and clusters act as superparamagnetic independent entities. A way to estimate the interparticle interactions is to plot $1/\chi$ vs T in the superparamagnetic regime. $1/\chi$ follows a Curie-Weiss-like law:

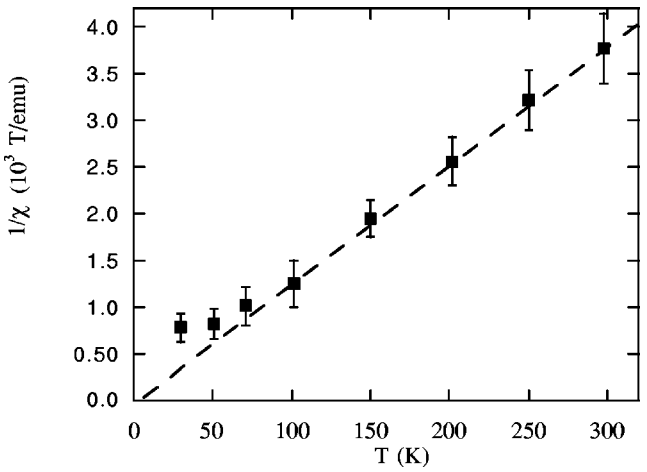

FIG. 2. Inverse of the sample susceptibility plotted versus the temperature T, making a linear extrapolation of this curve for high temperatures, one obtains, when $1/\chi\rightarrow 0$, an idea of the interaction temperature: $\theta=1-2$ K.

$$\frac{1}{\chi}=C(T-\theta) \tag{1}$$

and θ gives an order of magnitude of the particle interactions.[21] From experimental data, we give $1/\chi$ vs T in Fig. 2, and find $\theta=1-2$ K, which is negligible compared with the other energies of the clusters. In the superparamagnetic regime, we also estimate in Sec. IV A the magnetic size distribution of the clusters. At low temperatures, clusters have a ferromagnetic behavior due to the anisotropy terms. And, in Sec. IV B, we experimentally estimate their mean anisotropy constant.

A. Magnetic size measurement

In the following, we make the approximation that the atomic magnetic moment is equal to $1.7\mu_B$ at any temperature (or 1430 emu/cm^3 like in the bulk hcp cobalt). Besides, our synthesized cobalt clusters have approximately a 3-nm diameter and contain at least 1000 atoms. According to Refs. 22 and 23, a magnetic moment enhancement only appears for particles containing less than 500 atoms. So in our size range we can assume that the atomic cobalt moment is close to the bulk phase one ($m_{Co}=1.7\mu_B$). We consider a log-normal size distribution:

$$f(D)=\frac{1}{D\sqrt{2\pi\sigma^2}}\exp\left\{-\left[\ln\left(\frac{D}{D_m}\right)\right]^2\frac{1}{2\sigma^2}\right\}, \tag{2}$$

where D_m is the mean cluster diameter and σ the dispersion. In the superparamagnetic regime, we can use a classical Langevin function $L(x)$ and write

$$\frac{m(H,T)}{m_{sat}}=\frac{\int_0^\infty D^3L(x)f(D)\,dD}{\int_0^\infty D^3f(D)\,dD},\quad x=\frac{\mu_0H(\pi D^3/6)M_S}{k_BT}, \tag{3}$$

where H is the applied field (μ_0H in tesla), T the temperature, and m_{sat} the saturation magnetic moment of the sample

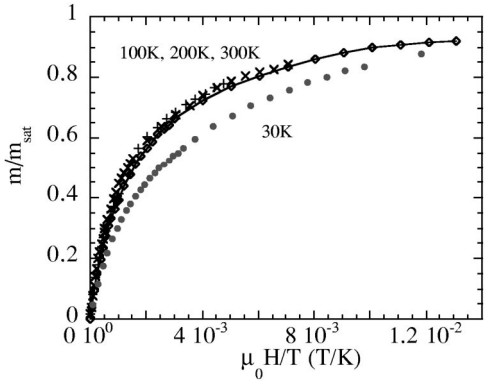

FIG. 3. In the superparamagnetic regime, $m(H/T)$ curves superimpose for $T=100$, 200, and 300 K. (+: 300 K; ×: 200 K; ◇: 100 K). At $T=30$ K (●: 30 K), the anisotropy energy is no more negligible, and one has to use a modified Langevin function to fit the curve.

estimated on magnetization curves at low temperatures under a 2-T field. First of all, in Fig. 3, one can see that for $T>100$ K, $m(H/T)$ curves superimpose according to Eq. (3) for a magnetic field being applied in the sample plane (we checked that the results are the same for a perpendicular applied field). Second, one can notice that for $T=30$ K, the magnetization deviation to the high-temperature curves comes from the fact that the anisotropy is not negligible anymore, and one has to use a modified Langevin function in the simulation.[24] In this equation, we also assume that the particles interact with the applied field. In fact, they interact with the local field which is the sum of the external field and the mean field created by the surrounding particles in the sample. Furthermore, in the superparamagnetic regime, we fit experimental $m(H,T)$ curves obtained from VSM measurements to find D_m and σ, the mean diameter and dispersion of the ''magnetic size'' distribution, respectively (see Fig. 4). For those fits, we still use the M_S bulk value [the use of other ones given in Refs. 25–27 leads quite to the same results (with an error less than 5%), the determining factors being D_m and σ]. Figure 5 displays D_m and σ for two niobium deposition rates ($F_{Nb}=3$ Å /s and $F_{Nb}=5$ Å /s, respectively). Such results are compared with the real cluster

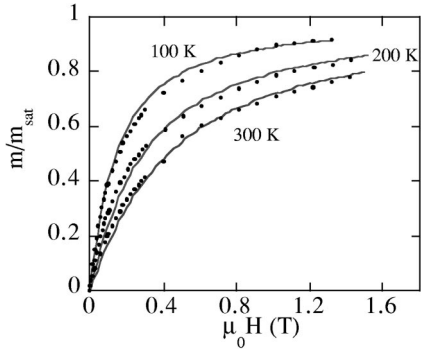

FIG. 4. We use a classical Langevin function to fit experimental magnetization curves $m(H)$ in the superparamagnetic regime (●: experimental data; continuous lines: fits). This allows us to deduce the mean particle diameter D_m and the dispersion σ of the magnetic size distribution considering a log-normal distribution for cobalt clusters.

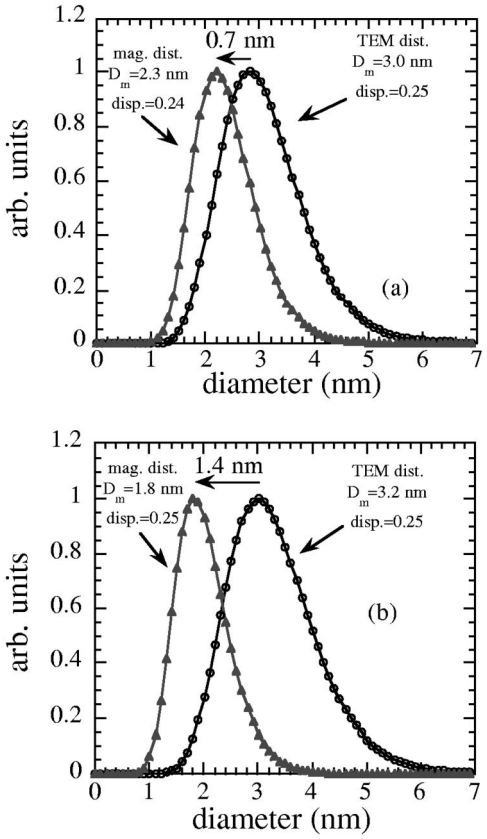

FIG. 5. (a) TEM size distribution: $D_m=3.0\pm0.1$ nm, $\sigma=0.24\pm0.01$ and magnetic size distribution: $D_m=2.3\pm0.1$ nm, $\sigma=0.24\pm0.01$ for a niobium deposition rate $F_{Nb}=3$ Å /s and a log-normal distribution, (b) TEM size distribution: $D_m=3.2\pm0.1$ nm, $\sigma=0.25\pm0.01$ and magnetic size distribution: $D_m=1.8\pm0.1$ nm, $\sigma=0.25\pm0.01$ for a niobium deposition rate $F_{Nb}=5$ Å /s.

sizes deduced from TEM observations. The magnetic domain is always smaller than the real diameter. Furthermore, the magnetic domain decreases as the deposition rate increases. This indicates that the kinetics of the deposition plays a crucial role for the nature of the interface. For example, we found a magnetic domain size of 2.3 nm (resp. 1.8 nm) for a 3-nm-diameter cluster when $F_{Nb}=3$ Å /s (resp. $F_{Nb}=5$ Å /s), the dispersion $\sigma=0.24$ remained the same.

B. Anisotropy

The bulk value of the fcc cobalt cubic magnetocrystalline anisotropy constant is: $K_{MA}=2.7\times10^6$ erg/cm^3 (Ref. 28) less than the hcp bulk phase one (4.4×10^6 erg/cm^3). The shape anisotropy constant K_{shape} can be calculated from the demagnetizing factors and the saturation magnetization. In case of weak distortions in the sphericity, the shape anisotropy for a prolate spheroid can be expressed as follows:

$$E_{shape}=\frac{1}{2}\mu_0 M_S^2(N_z-N_x)\cos^2(\theta)=K_{shape}\cos^2(\theta). \quad (4)$$

M_S is the saturation magnetization of the particle: $M_S=1430$ emu/cm^3, θ the angle between the magnetization direction and the easy axis, and N_x, N_z the demagnetizing factors along x axis and z axis, respectively. We plot in Fig. 6 the constant anisotropy K_{shape} as a function of the prolate

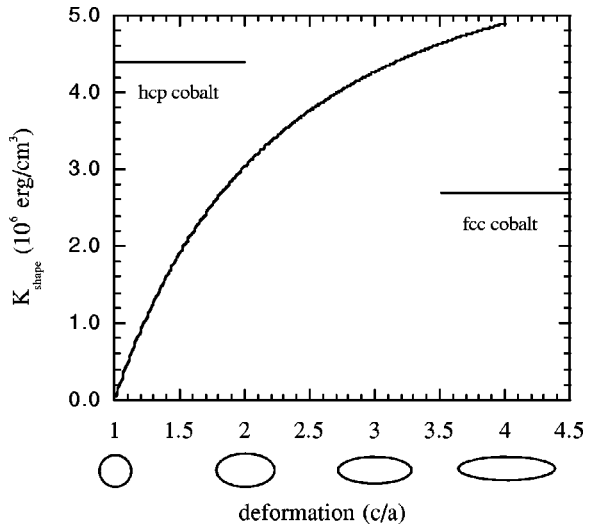

FIG. 6. The volumic shape anisotropy energy (K_{shape} in erg/cm^3) is plotted (continuous line) vs the particle deformation c/a assuming it is a prolate spheroid. We also report volumic magnetocrystalline anisotropy energy for fcc and hcp cobalt.

spheroid deformation c/a (Ref. 29) (with c and a representing the long and short ellipsoid axis, respectively). For a truncated octahedron, the ratio c/a has been evaluated lower than 1.2 which restricts the K_{shape} value of the order of 10^6 erg/cm^3. However, we have no information about the magnitude of interface and strain anisotropies in our system.

Let us now experimentally evaluate the anisotropy constant K_{eff} of cobalt clusters from low-temperature measurements. Hysteresis curves are obtained from VSM experiments, but at very low temperatures (i.e., $T<8$ K), superconducting fluctuations appear due to the niobium matrix and prevent any magnetization measurements on the whole sample. So, we also use x-ray magnetic circular dichroism as a local magnetometer by recording the MCD signal at the cobalt L_3 white line as a function of the applied magnetic field (for details on the method, see Ref. 30). The angle of the incident beam is fixed at 55° with respect to the surface normal and the magnetic field is parallel to the sample surface. The absorption signal is recorded by monitoring the soft x-ray fluorescence yield chosen for its large probing depth (1000 Å). Finally, from hysteresis curves given by both VSM and XMCD techniques, we deduce $m_r(T)$, the remanent magnetic moment vs T down to 5.3 K, and we normalize it by taking: $m_r(8.1\ \mathrm{K})_{VSM} = m_r(8.1\ \mathrm{K})_{XMCD}$, the curve $m_r(T)/m_r(5.3\ \mathrm{K})$ is given in Fig. 7. To evaluate $m_r(T)$, one can write

$$m_r(T) = \frac{m_{sat}}{Cte} \frac{\int_{D_B(T)}^{\infty} D^3 f(D)\, dD}{\int_0^{\infty} D^3 f(D)\, dD}, \tag{5}$$

where $D_B(T)$ is the particle blocking diameter at temperature T. Cte is a parameter independent of the particle size. $Cte = 2$ if clusters have a uniaxial magnetic behavior and $3 - \sqrt{3}$ if they have a cubic magnetic one. In order to rule out this Cte, we plot the ratio

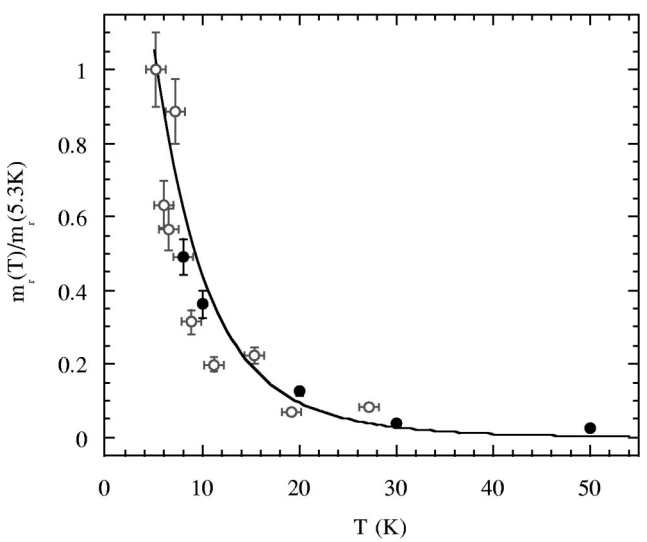

FIG. 7. Remanent magnetic moment plotted vs the temperature T. The signal is first normalized writing: $m_r(8.1\ \mathrm{K})_{VSM} = m_r(8.1\ \mathrm{K})_{XMCD}$, and then we take $m_r(5.3\ \mathrm{K}) = 1$. We see that the continuous line curve fits both VSM (●) and XMCD (○) measurements. From this fit, we can deduce the anisotropy constant K_{eff}.

$$\frac{m_r(T)}{m_r(5.3\ \mathrm{K})} = \frac{\int_{D_B(T)}^{\infty} D^3 f(D)\, dD}{\int_{D_B(5.3\ \mathrm{K})}^{\infty} D^3 f(D)\, dD}. \tag{6}$$

One finds $D_B(T)$ when the relaxation time of the particle is equal to the measuring time: $\tau = \tau_0 \exp(K_{eff} V/k_B T) = \tau_{\mathrm{mes}}$.

$$D_B^3(T) = aT, a = \frac{6k_B}{\pi K_{eff}} \ln\left(\frac{\tau_{mes}}{\tau_0}\right); \tag{7}$$

τ_0 is the microscopic relaxation time of the particle, taken independent of the temperature. The fit result is presented in Fig. 7. We find $a = 3.5 \pm 0.1$ nm^3/K, and by taking $\tau_{mes} = 10$ s, and $\tau_0 = 10^{-12}$–10^{-9} s, we obtain $K_{eff} = 2.0 \pm 0.3 \times 10^6$ erg/cm^3. By fitting zero-field cooled (ZFC) curves for different applied fields, we can also evaluate K_{eff}. Besides, if we neglect the blocked particle susceptibility, we have

$$\frac{m_{ZFC}(H,T)}{m_{sat}} = \frac{\int_0^{D_B(H,T)} D^3 L(x) f(D)\, dD}{\int_0^{\infty} D^3 f(D)\, dD}. \tag{8}$$

Moreover, for low-field values compared with the anisotropy field of cobalt clusters (estimated to be $\mu_0 H_a = 0.4$ T), we can make the approximation

$$D_B^3(H,T) = af\left(\frac{H}{H_a}\right) T \approx a\left(1 + \alpha \frac{H}{H_a}\right) T, \tag{9}$$

where a is the coefficient of Eq. (7), α a numerical constant. The ZFC curve fits are presented in Fig. 8. A linear extrapolation to $\mu_0 H = 0$ T also gives $a \approx 3.5$ nm^3/K and an anisotropy constant of $2.0 \pm 0.3 \times 10^6$ erg/cm^3 for the same numerical values as above. We found a similar result for the second

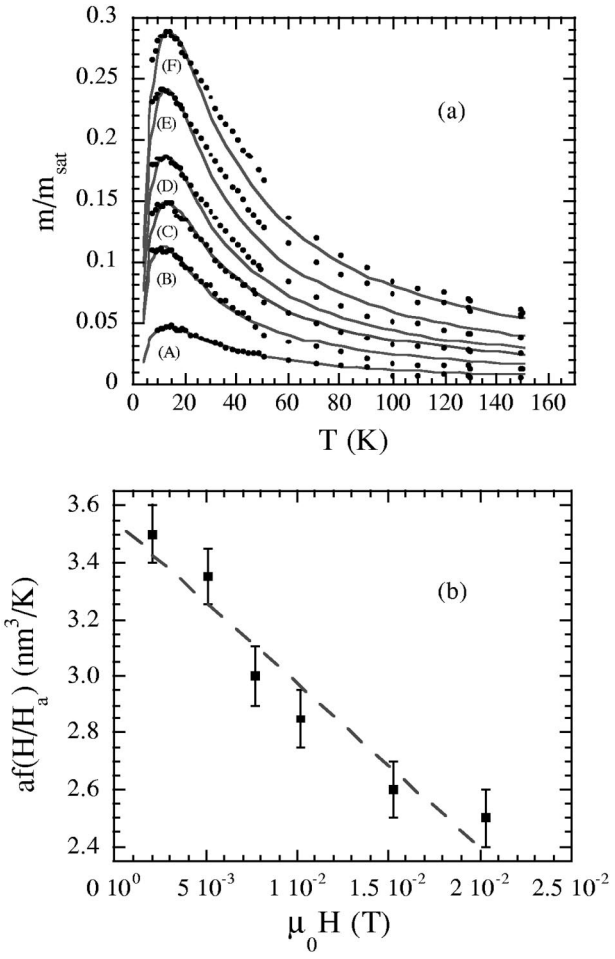

FIG. 8. (a) ZFC curves (black dots) taken for six different applied fields: (a) 0.002 T, (b) 0.005 T, (c) 0.0075 T, (d) 0.01 T, (e) 0.015 T, (f) 0.02 T. (b) Fits (continuous lines) allow us to deduce $af(H/H_a)$ $[D_B^3(H,T)=af(H/H_a)T]$ and then the anisotropy constant K_{eff}.

sample with a niobium evaporation rate of 5 Å /s. Finally, we experimentally found an anisotropy constant close to the one of quasispherical fcc cobalt clusters.

V. DISCUSSION

The ''magnetic size'' distribution is compared to the one obtained from TEM observations of pure Co clusters prepared in the same experimental conditions [see Fig. 5(a)]. For all the studied Co/Nb samples, we systematically find a global size reduction which might be related to the formation of a nonmagnetic alloy at the interface as suggested by EXAFS simulations. The most significant parameter in the magnetically dead alloy thickness seems to be the rate of deposition of the niobium matrix (F_{Nb}). As an example, we mention that for $F_{Nb}=5$ Å /s, the reduction is twice the one for $F_{Nb}=3$ Å /s [see Fig. 5(b)]. That result suggests the model proposed in Figs. 9(a) and 9(b). As cobalt niobium forms a miscible system,[31] we show that the more F_{Nb} increases, the more the quantity of Nb atoms introduced at the cobalt cluster surface increases.

To study the magnetism of the perturbed monolayers at the interface, we prepared a cobalt-niobium alloy using induction heating under argon atmosphere with 40%-Co and 60%-Nb atomic weights. From classical x-ray $\theta/2\theta$ diffraction ($\lambda=1.5406$ Å), we identified the β phase given by the binary phase diagram: Co_6Nb_7. From VSM measurements on this sample, we found a remaining paramagnetic susceptibility $\chi=10^{-4}$ (for $2<T<300$ K) corresponding to the ''Pauli'' paramagnetism of the sample. This feature could explain the ''dead'' layer at the cluster surface. Obi *et al.*[32] obtained two ''magnetically dead'' cobalt monolayers on cobalt-niobium multilayers evaporated by a rf-dual-type sputtering method (magnetically dead layers were also suggested by Mühge *et al.*[33] for Fe/Nb multilayers). Finally, we can underline the fact that the preformed cobalt clusters by LECBD technique are very compact nanocrystallites which conserve a magnetic core even if embedded in a miscible matrix. The existence of a magnetically dead layer at the cluster-matrix interface may reduce surface effects compared with recent results obtained on smaller cobalt particles (150–300 atoms) stabilized in polymers.[23] The estimated mean anisotropy constant might correspond to cubic magnetocrystalline or shape effects. To confirm this assumption, works are in progress to investigate the magnetic properties of a single cluster in a niobium matrix using a new micro-SQUID technique.

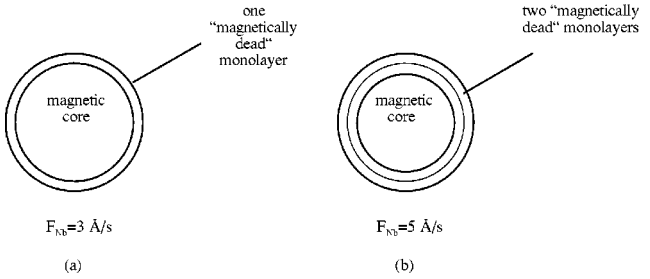

FIG. 9. (a) Expected magnetic structure of cobalt clusters embedded in a niobium matrix, we find one magnetically dead cobalt monolayer (2×3.5 Å in diameter) for a $F_{Nb}=3$ Å /s deposition rate, (b) two magnetically dead cobalt monolayers (4×3.5 Å in diameter) are found for $F_{Nb}=5$ Å /s.

One can also mention that for XMCD signals detected from the total electron yield method, the extraction of quantitative local magnetic values from the applicability of the individual orbital and spin sum rules is in progress.[34] Nevertheless, one can mention a small enhancement of the orbital/spin magnetic moment ratio.[34] Such increase might come from the orbital magnetic moment enhancement expected for small particles.[27] Systematic XMCD studies on clusters assembled Co/*X* films should be performed on Si-protected layers under synchrotron radiation to confirm these results.

VI. CONCLUSION

We have shown that the magnetic properties of nanoparticles can be evaluated unambiguously if we know the size, the shape, and the nature of the interface. This latter is given by EXAFS spectroscopy. We summarize the main results:

(i) The mean-like-bulk Co-Co distance ($d_{Co-Co}=2.50$ Å) concerns the 3/4 of the atoms (namely, the core atoms).

(ii) Co-Nb bonds are located on roughly one monolayer at the surface of the Co clusters embedded in the Nb matrix.

Even though this interface is rather sharp, it is of impor-

tance since the interface thickness is on the same order of magnitude as the cluster radius. In addition, some magnetic properties were approached by different complementary techniques as VSM magnetometry (at temperatures higher than 8 K) and XMCD signal detected by the fluorescence yield method (at temperatures from 5.3 to 30 K) under a magnetic field. We show the good result coherence on the superimposed range ($8<T<30$ K) for both techniques probing the whole thickness of the sample. The main result is the possibility of a magnetically dead layer at the interface Co/Nb, to relate to the alloyed interface (from EXAFS measurements) and to the moderate anisotropy value (found around 2×10^6 erg/cm^3). To confirm this assumption and to understand the role of the interface on the anisotropy terms involved in so low dimension magnetic nanostructures, XMCD measurements at the Co-$L_{2,3}$ edge have to be provided on a Co/Nb bilayer stacking (alternating two monolayers of Co and two monolayers of Nb) with the same Nb-deposition rates as in our systems.

ACKNOWLEDGMENTS

The authors would like to thank M. Negrier and J. Tuaillon for fruitful discussions, C. Binns from the University of Leceister, United Kingdom and J. Vogel from the Laboratoire Louis Néel at Grenoble, France for their help during the first XMCD tests on the ID12B line of N. Brookes at the ESRF in Grenoble.

[1] T. Chang, J. G. Zhu, and J. H. Judy, J. Appl. Phys. **73**, 6716 (1993).
[2] A. K. Geim, S. V. Dubonos, J. G. S. Lok, I. V. Grigorieva, J. C. Maan, L. Theil Hansen, and P. E. Lindelof, Appl. Phys. Lett. **71**, 2379 (1997).
[3] W. Wernsdorfer, E. Bonet Orozco, K. Hasselbach, A. Benoit, B. Barbara, N. Demoncy, A. Loiseau, H. Pascard, and D. Mailly, Phys. Rev. Lett. **78**, 1791 (1997).
[4] F. Parent, J. Tuaillon, L. B. Steren, V. Dupuis, B. Prével, P. Mélinon, A. Pérez, G. Guiraud, R. Morel, A. Barthélémy, and A. Fert, Phys. Rev. B **55**, 3683 (1997).
[5] P. Milani and W. A. de Heer, Rev. Sci. Instrum. **61**, 1835 (1990).
[6] A. Pérez, P. Mélinon, V. Dupuis, P. Jensen, B. Prével, M. Broyer, M. Pellarin, J. L. Vialle, and B. Palpant, J. Phys. D **30**, 1 (1997).
[7] M. Pellarin, E. Cottancin, J. Lermé, J. L. Vialle, J. P. Wolf, M. Broyer, V. Paillard, V. Dupuis, A. Pérez, J. P. Pérez, J. Tuaillon, and P. Mélinon, Chem. Phys. Lett. **224**, 338 (1994).
[8] M. Négrier, J. Tuaillon, V. Dupuis, P. Mélinon, A. Pérez, and A. Traverse (unpublished).
[9] J. Tuaillon, V. Dupuis, P. Mélinon, B. Prével, M. Treilleux, A. Pérez, M. Pellarin, J. L. Vialle, and M. Broyer, Philos. Mag. A **76**, 493 (1997).
[10] F. Baudelet, A. Fontaine, G. Tourillon, D. Gay, M. Maurer, M. Piecuch, M. F. Ravet, and V. Dupuis, Phys. Rev. B **47**, 2344 (1993).
[11] J. Mimault, J. J. Faix, T. Girardeau, M. Jaouen, and G. Tourillon, Meas. Sci. Technol. **5**, 482 (1994).
[12] B. Carriere and G. Krill, Mater. Sci. Forum **59**, 221 (1990).
[13] A. G. McKale, G. Sknapp, and S. K. Chan, Phys. Rev. B **33**, 841 (1986).
[14] A. Michalowicz and N. Allali, J. Phys. IV **7**, C2-261 (1997).
[15] M. Roy, J. Phys. IV **C2**, 151 (1997).
[16] E. Prouzet, A. Michalowicz, and N. Allali, J. Phys. IV **7**, C2-261 (1997).
[17] V. Dupuis, M. Maurer, M. Piecuch, M. F. Ravet, J. Dekoster, S. Andrieu, J. F. Bobo, F. Baudelet, P. Bauer, and A. Fontaine, Phys. Rev. B **48**, 5585 (1993).
[18] Š. Pick and H. Dreyssé, J. Magn. Magn. Mater. **198**, 312 (1999).
[19] R. V. Hardeveld and F. Hartog, Surf. Sci. **15**, 189 (1969).
[20] The anisotropy constant used for this calculation is given in Sec. IV B.
[21] J. L. Dormann, D. Fiorani, and E. Tronc, in *Advances in Chemical Physics*, edited by I. Prigogine and Stuart A. Rice (Wiley, New York, 1997), Vol. XCVIII, p. 283.
[22] I. M. L. Billas, A. Chatelain, and W. A. de Heer, Science **265**, 1682 (1994).
[23] M. Respaud, J. M. Broto, H. Rakoto, A. R. Fert, L. Thomas, and B. Barbara, Phys. Rev. B **57**, 2925 (1998).
[24] K. Müller and F. Thurley, Int. J. Magn. **5**, 203 (1973).
[25] P. Bruno, Ph.D. thesis, Paris Orsay, France, 1989.
[26] M. Alden, S. Mirbt, H. L. Skriver, N. M. Rosengaard, and B. Johansson, Phys. Rev. B **46**, 6303 (1992).
[27] J. Dorantes-Davila, H. Dreyssé, and G. M. Pastor, Phys. Rev. B **55**, 15 033 (1997).
[28] J. P. Chen, C. M. Sorensen, K. J. Klabunde, and G. C. Hadjipanayis, J. Appl. Phys. **76**, 6676 (1994).
[29] A. Aharoni, *Introduction to the Theory of Ferromagnetism* (Oxford Science Publications, New York, 1996), p. 116.
[30] C. T. Chen, Y. U. Idzerda, H.-J. Lin, G. Meigs, A. Chaiken, G. A. Prinz, and G. H. Ho, Phys. Rev. B **48**, 642 (1993).
[31] T. B. Massalski, J. L. Murray, L. H. Bennett, and H. Baker, *Binary Phase Diagrams* (American Society for Metals, Metals Park, OH).
[32] Y. Obi, M. Ikebe, T. Kubo, and H. Fujimori, Physica C **317-318**, 149 (1999).
[33] Th. Mühge, K. Westerholt, H. Zabel, N. N. Garifyanov, Yu. V. Goryunov, I. A. Garifullin, and G. G. Khaliullin, Phys. Rev. B **55**, 8945 (1997).
[34] C. T. Chen, Y. U. Idzerda, H.-J. Lin, N. V. Smith, G. Meigs, E. Chaban, G. H. Ho, E. Pellegrin, and F. Sette, Phys. Rev. Lett. **75**, 152 (1995).